Boltzmann Statistics Rotational-Echo Double-Resonance Analysis

ARTICLE *in* THE JOURNAL OF PHYSICAL CHEMISTRY B · AUGUST 2007

Impact Factor: 3.3 · DOI: 10.1021/jp072504q · Source: PubMed

Boltzmann Statistics Rotational-Echo Double-Resonance Analysis

John D. Gehman,[†] Frances Separovic,[†] Kun Lu,[‡] and Anil K. Mehta*[,‡]

School of Chemistry, Bio21 Institute, University of Melbourne, Melbourne, Victoria 3010, Australia, and Department of Chemistry, Emory University, Atlanta, Georgia 30322

Received: March 30, 2007

A new approach to rotational-echo double-resonance (REDOR) data analysis, analogous to Boltzmann maximum entropy statistics, is reported. This Boltzmann statistics REDOR (BS-REDOR) approach is useful for reconstructing an unbiased internuclear distance distribution for multiple internuclear distances from experimentally limited REDOR data sets on isolated spin pairs. The analysis is characterized by exploring reconstructions on model data and applied to both [1-^{13}C,^{15}N]-glycine and a long intramolecular distance in Aβ (16−22) peptide nanotubes. The approach also provides insight into the minimal number of REDOR data points required to allow faithful determination of dipolar couplings in systems with multiple internuclear distances.

Introduction

Solid-state NMR has rapidly emerged as a strong complement to X-ray diffraction and solution NMR in structural biophysics. In particular, rotational-echo double-resonance (REDOR)[1,2] has proven to be a powerful and robust method to address structure by measuring internuclear distances from dipolar couplings in proteins,[3,4] peptides,[5−10] membrane-bound peptides and proteins,[11−16] complexes,[17−26] insoluble aggregates,[27−29] and materials.[30−33]

Magic-angle spinning (MAS)[34,35] provides high-resolution solid-state NMR spectra but removes detailed structural information. REDOR allows measurement of internuclear distances by reintroducing the heteronuclear (I−S) dipolar coupling with rotor synchronized π pulses every half-rotor period during MAS. The reintroduced dipolar coupling causes the observe S spin to dephase faster than when subject only to transverse (T_2) relaxation processes. The ratio of signal obtained with (S) and without (S_0) the dephasing π pulses is a function of the heteronuclear dipolar coupling, itself a simple function of the internuclear distance. In samples containing ^{13}C and ^{15}N nuclei, accurate measurements of distances out to 6 Å can provide detailed structural information. Even longer internuclear distances can be measured using nuclei with higher gyromagnetic ratios. A typical REDOR experiment consists of a measured S/S_0 (or $1 - S/S_0$) for a series of dephasing times, extending to tens of milliseconds (Figure 1) until the full-echo signal S_0 is lost to natural T_2 processes.

The development of stronger NMR magnetic fields has increased sensitivity and substantially expands the utility of REDOR, as it allows atomic-level measurements on smaller amounts of sample. While many of these samples inherently have a distribution of distances, current REDOR analysis methods are restricted in their potential to determine these distances and distributions. These methods vary in complexity, but were greatly simplified by the advent of an analytic approximation of the REDOR curve.[36] This allowed for rapid fitting of isolated spin-pairs each with a single I−S distance.[3,37] Similarly, more complicated but mutually exclusive distributions have been simulated and compared to the data to differentiate between conceivable structural models.[26,38−40]

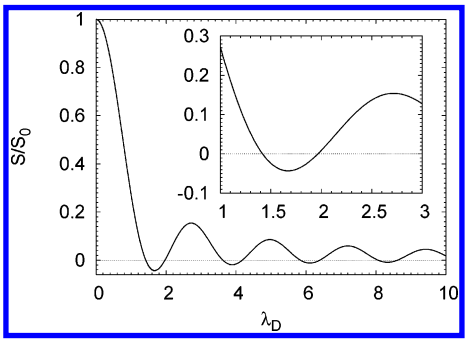

Figure 1. Universal REDOR dephasing curve plotted as a function of the unitless parameter $\lambda_D = DN_cT_r$.

Ideally, analysis of REDOR data would not involve the bias of a supposed functional form for the distance distribution. To this end, Fourier transformation has been explored to produce a free-form dipolar coupling spectrum.[2,41,42] An impressive advance was made with REDOR transforms,[41,43] which use Bessel functions or more customized expressions as the kernel to deconvolute a REDOR curve into component dipolar couplings. The REDOR transform has measured ^{13}C−^{15}N dipolar couplings in peptides,[44] using the equivalent of just 600 μg of ^{13}C-labeled sample. However, even with 28 REDOR data points, the resolution in the dipolar coupling spectrum was limited by the finite sampling rate and total dephasing time. Further progress in REDOR data processing, which compares the REDOR transform to other approaches for "ill-posed problems",[45] have been reported.[46] Asymptotic rescaling as well as Tikhonov regularization appear to be as good or better for handling data with finite error. Similar to Fourier transform of indirect dimensions of multidimensional NMR spectra, spectral resolution of the REDOR transform and regularization methods depend on sampling frequency and relatively long "acquisition times". Limited experimental time constrains the maximum signal-to-noise that can be achieved at each data point. Limited

* Author to whom correspondence should be addressed. Phone: +1 404 727 2610. Fax: +1 404 727 6596. E-mail: anil.mehta@emory.edu.
† University of Melbourne.
‡ Emory University.

10.1021/jp072504q CCC: $37.00
Published on Web 06/21/2007

signal-to-noise is particularly acute for the longer REDOR evolution times owing to T_2 relaxation. Consequently, REDOR experiments typically include fewer but higher signal-to-noise data points at relatively short evolution times, forfeiting the ability to perform an unbiased deconvolution of dipolar couplings with the above methods and instead fit to a preconceived distance distribution. At an extreme, the current world record is 3 months of acquisition for a single REDOR point.[20]

In this article we develop a REDOR processing scheme which employs maximum entropy Boltzmann statistics to determine an unbiased distribution of internuclear distances with the advantage that only REDOR data collected at relatively short dephasing times (where data error is least significant), as are often collected in typical biological solid-state NMR samples, are required. Our Boltzmann statistical approach differs significantly from previous applications of maximum entropy for reconstruction of power spectra from time domain signals,[47,48] $^{15}N-^{1}H$ heteronuclear dipolar coupling in PISEMA spectra[49] and REDOR data.[46] As detailed below, these use an adaptation of Shannon's entropy[50] as a "regularization functional" to be maximized.

Experimental Methods

REDOR as an Inverse Problem. The time-dependent REDOR dephasing signal for a heteronuclear spin pair with isotropically distributed internuclear vectors is a double integral over azimuthal and polar angles α and β between the internuclear vector and the rotor spinning axis

$$\left(\frac{S}{S_0}\right) = \int_0^{\pi}\int_0^{2\pi} d\alpha \sin(\beta)\, d\beta \cos[2\sqrt{2}\lambda_D \sin(2\beta)\sin(\alpha')] \tag{1}$$

where $\alpha' = \alpha + 2\pi\phi$ for a π pulse centered at fraction ϕ of every rotor period, and $\lambda_D = DN_cT_r$ for number of rotor periods N_c, MAS speed $1/T_r$, and dipolar coupling constant $D = \mu_0\hbar\gamma_I\gamma_S/(8\pi^2r^3)$ for internuclear distance r.[41,51,52] REDOR data plotted in terms of the unitless time index λ_D for fixed $\phi = 0.5$ results in the universal REDOR curve[1,36,51] (Figure 1). This allows REDOR curves to be described in frequency-independent, generalized terms. For example, significant dephasing is found at time $1/D$ where $\lambda_D = 1$, and S/S_0 for all frequencies is negative between zero-crossings at $\lambda \simeq 1.4$ and 1.96, reaching a minimum value at $\lambda_D \simeq 1.67$.

For each isolated heteronuclear spin-pair with a distribution of internuclear distances r_i, and fractional densities n_i (normalized to 1), the contribution to the observed REDOR dephasing is simply a population-weighted sum of terms

$$\frac{S}{S_0} = \sum_i n_i\left(\frac{S}{S_0}\right)_i \tag{2}$$

In the REDOR experiment, T_r and ϕ are fixed, and observe nucleus dephasing is calculated as a function of time $N_c{\cdot}T_r$. For several internuclear distances r_i with corresponding dipolar coupling constants D_i, only the I fractional probabilities n_i are needed to calculate dephasing curves at each of J time points. The REDOR data can consequently be described by

$$\left(\frac{S}{S_0}\right)_j = \sum_i \mathscr{R}_{ij}n_i \tag{3}$$

where

$$\mathscr{R}_{i,j} = \frac{\pi}{\Omega^2}\sum_{b=0}^{\Omega}\sum_{a=0}^{2\Omega}\sin(\beta)\cos[2\sqrt{2}\lambda_D\sin(2\beta)\sin(\alpha')] \tag{4}$$

with $\lambda_D = D_i(N_c)_jT_r$, $\alpha = \pi a/\Omega$, $\beta = \pi b/\Omega$, and Ω is the number of discrete points per π radians used to digitize the integrals in eq 1. Cast this way, $\mathscr{R}$ is simply a matrix of I basis set functions, each being a REDOR curve calculated for given internuclear distance r_i over a series of rotor periods $(N_c)_j$. The data then is simply a linear combination of these basis set functions, the coefficients $\vec{\mathbf{n}} = \{n_i\}$ for which are what we wish to find. This form is helpful when it is appropriate to specify a priori a functional form for the distribution of internuclear distances $\vec{\mathbf{n}}$, as analytic derivatives are straightforward and REDOR curves for trial distributions are easily calculated. Equation 3 also serves as the premise for maximum entropy reconstruction.

Boltzmann Statistics REDOR (BS-REDOR) Analysis. Our REDOR maximum entropy approach is similar to the derivation of Boltzmann's distribution for particles distributed over many energy states. Bevensee[53] provides an excellent guide for the general application of this formalism. In the present case, an ensemble of N spin-pairs with internuclear distance r_i is distributed among different but equally probable states $\{N_i\} = \{N_1, N_2, ..., N_i, ... N_I\}$, where $N = \sum_i N_i$. For distinguishable spin-pairs, the "entropy" H of a given state $\{N_i\}$ is defined as

$$H \equiv \ln\frac{N!}{\Pi\, N_i!} \tag{5}$$

Maximizing the entropy H reveals the most probable radial distribution function $\{N_i\}$.

However, it is not just the most probable distribution of internuclear distances that is important, but the most probable distribution consistent with the REDOR data. Hence, constraints must be added to eq 5 using the method of Lagrange multipliers, thereby building an objective function which is maximal only when the constraints are satisfied. A self-evident constraint is given by normalizing the fractional densities n_i, and additional constraints are provided at each experimental REDOR data point j by eq 3. For simplicity the spin-pair population is normalized to the total population via $n_i = N_i/N$. While the precision used to express $\{n_i\}$ defines the effectual value of N assumed, typical precisions are sufficient that Stirling's approximation may be used to simplify the entropy component from eq 5

$$H^{\mathrm{REDOR}} = -\sum_i n_i \ln\left(n_i\right) + \lambda_0\left(\sum_i n_i - 1\right) + \sum_j \lambda_j\left(\sum_i \mathscr{R}_{ij}n_i - \left(\frac{S}{S_0}\right)_j\right) \tag{6}$$

The principal difference between this objective function and existing maximum entropy approaches is the presence of the second term and the means of constraining the process with the data in the third term; existing approaches use a single Lagrange multiplier which scales a root-mean-square deviation between the reconstruction and all data points. Zeroing the partial derivatives $\partial(H^{\mathrm{REDOR}})/\partial n_i$ provides for extremes of the function, which are a maximum and not a minimum as $\partial^2(H^{\mathrm{REDOR}})/\partial n_i^2 < 0$. Solving for n_i, and summing over all i together with the normalization $\sum_i n_i = 1$ provides the partition

function such that

$$n_i = \frac{\prod_j e^{\lambda_j \mathscr{R}_{ij}}}{\sum_i \left(\prod_j e^{\lambda_j \mathscr{R}_{ij}} \right)} = \frac{\exp\left\{ \sum_j \lambda_j D_{ij} \right\}}{\sum_i \exp\left\{ \sum_j \lambda_j D_{ij} \right\}} \tag{7}$$

or in matrix form

$$\vec{\mathbf{n}} = \frac{\exp\{\mathscr{R}^{\mathrm{T}} \vec{\lambda}\}}{(\exp\{\mathscr{R}^{\mathrm{T}} \vec{\lambda}\}) \cdot \vec{\mathbf{1}}} \tag{8}$$

where the exponential of a vector is defined as the vector of the exponential of each of the vector elements, and $\vec{\mathbf{1}}$ is unity at each element, and with dimensionality *I*. For convenience we cast the partition coefficient as *Z*, and numerators as $\vec{\imath}$. Equations 3 and 7 provide a system of *J* nontrivial equations in *J* unknowns, the Lagrange multipliers λ_j

$$\overrightarrow{\mathbf{S}/\mathbf{S}_0} = \frac{1}{Z} \mathscr{R} \vec{\imath} \tag{9}$$

When an unbiased and continuous distribution of internuclear distances is present, it is likely that $I \gg J$; i.e., the number of discrete distances used in approximating the continuous distribution will be much greater than the number of measured REDOR data points. Equation 9 effectively reduces an *I*-dimensional constrained optimization into a *J*-dimensional unconstrained problem.

Lagrange Multipliers. The REDOR dephasing curve calculated from a configuration *q* of Lagrange multipliers $\vec{\lambda}_q$ and described by points $(S/S_0)_{j_q}$ is assessed against the data to give a goodness-of-fit χ_q^2 via

$$\chi_q^2 = \sum_j \frac{1}{\sigma_j^2} [(S/S_0)_{j_q} - (S/S_0)_j]^2 \tag{10}$$

This error is calculated from the sums of S_0 (full-echo) and *S* (dephased) intensities of an MAS-modulated manifold of *P* peaks and baseline root-mean-square (rms) noise σ_{S_0} and σ_S

$$\sigma_j \propto \sqrt{P} \frac{S}{S_0} \left\{ \left(\frac{\sigma_S}{S} \right)^2 + \left(\frac{\sigma_{S_0}}{S_0} \right)^2 \right\}^{1/2} \tag{11}$$

σ_j is set to unity for reconstructions on model data with no error, equally weighting all points. Scaling the rms of noise up by a factor of 2.5 will approximate spectral peak-to-peak noise,[54] and provide 99% confidence limits. As for experimental data presented below, peak heights may be used in lieu of peak integrals when S_0 and *S* linewidths are identical, thereby minimizing error. However, with peak integrals, *P* must be the total number of integrated points.

The configuration of Lagrange multipliers $\vec{\lambda}$ is optimized by minimizing χ^2. Straightforward nonlinear least-squares approaches to identify $\vec{\lambda}$ are highly dependent on the starting configuration, similar to previous experience.[48] Attempts to control the evolution of the nonlinear least-squares fit using suggested techniques[53] require difficult tuning for every different data set and are hence anything but robust.

We instead employ a simulated annealing approach which provides a more random but easily understood controlled search of $\vec{\lambda}$ configuration space, which is reasonably independent of the initial state.[55] Simulated annealing performs a prescribed number of steps at each temperature in a geometric cooling schedule. At each step, a random number within a prescribed range about zero is added to each Lagrange multiplier. If the "energy" χ_{q+1}^2 of configuration $\vec{\lambda}_{q+1}$ is lower than the previous iteration χ_q^2 at temperature *T*, the step is accepted. If the "energy" is higher, it is accepted with a probability of

$$\exp\{-(\chi_{q+1}^2 - \chi_q^2)/kT\} \tag{12}$$

for a prescribed "Boltzmann constant" *k*.

All analysis was implemented in C/C++ and compiled under SuSE 9.3 Linux using the GNU compiler (g++). The code makes extensive use of the freely available GNU Scientific Library, version 1.7,[56] specifically with respect to vector and matrix structures and operations, random number generators, and the simulated-annealing algorithm. On an Athlon XP2100+ 1.73 MHz processor, analysis using $I = 501$ discrete distances and $J = 11$ data points with 100 steps at each temperature takes approximately 12 s per 1000 temperature steps. Our implementation of BS-REDOR can be obtained as directed at http://www.chemistry.unimelb.edu.au/staff/fs/research/.

Monte Carlo Error Analysis. The finite signal-to-noise of peak heights or integrals lend error to the experimental REDOR data points. Using a Monte Carlo (MC) approach, similar to that used for noise analysis in rate matrix time reversal of exchange spectra,[57] the impact of random noise can be assessed. In each of hundreds of MC iterations, random values are added to each of the data points, and run through BS-REDOR again. The average and standard deviation statistics of n_i at each r_i over all MC reconstructions are calculated and used to assess the conceivable variation in distance distributions arising from Gaussian random error in the data.

Random numbers for MC analysis were selected from a Gaussian random distribution with standard deviation equal to the error in the data point σ_j as defined in eq 11. A Gaussian random number with normal distribution (mean zero and standard deviation 1.0) is generated by summing 12 random numbers with flat probability between 0 and 1, and subtracting 6.0.[58] This is multiplied by σ_j, then added to the corresponding data point $(S/S_0)_j$ for each MC iteration.

NMR. NMR measurements were made on a Bruker (Karlsruhe, Germany) Avance 600 spectrometer with a ^{13}C frequency of 150.8 MHz and ^{15}N frequency of 60.3 MHz using a Bruker 4 mm triple-resonance MAS probe. Transverse ^{13}C magnetization was prepared by 2 ms ^{1}H−^{13}C cross-polarization[59] with a 50 kHz ^{13}C spin-lock pulse and linear ^{1}H spin-lock ramp from 50 to 70 kHz. To compensate for pulse imperfections, xy8-REDOR[60,61] was implemented with π-pulses on ^{13}C and ^{15}N channels every rotor period and pulse widths of 6 μs and 10 μs, respectively. EXORCYCLE phase cycling was applied to the final ^{13}C Hahn-echo refocusing pulse before acquisition.[62,63] 95 kHz Spinal64[64] ^{1}H decoupling was used during both REDOR evolution and acquisition. To avoid phase twists resulting from detuning by ^{15}N pulse heating, 64 dummy scans preceded every spectrum, with full-echo (S_0) and dephased (*S*) spectra consecutively signal-averaged over 64 scans for glycine and 1024 scans for the nanotubes instead of the accepted method of alternating between *S* and S_0 every scan. MAS frequency was maintained at 8 kHz for glycine and 10 kHz for nanotubes, ±2 Hz using a Bruker MAS speed controller. Both spin rates provide for a rotor period of an integer length (125 and 100 μs, respectively). The slower spin rate removes complications caused by a rotational-resonance match condition[65] between glycine carbonyl and methylene carbons at 14.1 T, and the faster spin rate provides better signal-to-noise for the carbonyl carbon by reducing the number of sidebands. Glycine data was collected

at room temperature. To ensure that MAS and RF heating did not denature the Aβ(16−22) nanotubes the exit temperature of the cooling and spinning air was kept below −1 °C. ^{1}H−^{13}C and ^{1}H−^{15}N cross-polarization spectra taken before and after the REDOR experiment ensured that the sample did not change.

Aβ (16−22) Nanotubes. Labeled amino acids were purchased from CIL. ^{13}C- and ^{15}N-labeled N- and C-capped Aβ(16−22) (KLVFFAE) peptide was synthesized on a Rainin Symphony QUARTET multiplex solid-phase peptide synthesizer using standard NMM/HBTU protocols for Fmoc solid-phase synthesis. Peptides were purified by RP-HPLC. Final purity greater than 98% was confirmed by HPLC and molecular weight confirmed by MALDI-TOF using a 2,5-dihydroxybenzoic acid matrix. Purified peptide was dissolved in 40% acetonitrile/water (v/v) with 0.1% TFA (pH ≈ 2.1) to a final concentration of 1.3 mM and allowed to self-assemble and mature for 2 weeks. Nanotubes were precipitated with SO_4^{2-} in the presence of 30 mM trehalose, 0.67 mg/mL dextran (81.5 and 488 kDa), and 1% PEG-8000, which acted as cryo- and lyo-protectants during lyophilization. The presence of only intact tubes after lyophilization was confirmed by electron microscopy.

α-Glycine. 20.1 mg of [^{15}N,1-^{13}C]glycine (Aldrich, St. Louis, MO) was co-dissolved with 200.9 mg of natural abundance glycine (Aldrich) in 18 MΩ water and permitted to slowly evaporate. The subsequent α-glycine crystals were crushed and packed in a 4 mm MAS rotor.

Results and Discussion

Existing transform approaches to REDOR data[41,43,44,46] typically require apodized REDOR data extending to $\lambda_D = 15-30$. REDOR data at long evolution times is difficult to acquire when measuring non-trivial heteronuclear distances in typical biological samples owing to diminishing signal-to-noise. Typically data is collected only at shorter REDOR dephasing times ($\lambda_D \lesssim 2$), and the closest match to preconceived model distance distributions is determined. For the case of one or two distances, straightforward nonlinear least squares (NLLS) can analytically fit such data sets.[66]

The BS-REDOR approach is designed to find the most probable and unbiased distribution of distances consistent with the data and performs similarly to NLLS for a single discrete distance. Figure 2 shows a BS-REDOR reconstruction on model data calculated for a discrete ^{13}C−^{15}N 3 Å distance, using 10 evenly spaced data points extending to $\lambda_D = 2.9$. The BS-REDOR analysis correctly reports a very narrow distribution of distances centered at 3 Å.

Data Truncation. Figure 2 also explores the effect of aggressive truncation on reconstructions of a single discrete distance. Truncation to $\lambda_D \approx 1$, reducing the data to just three points, results in a Gaussian distribution of distances centered at the correct distance. The distribution of this Gaussian should be interpreted as the uncertainty in the distance measurement, in contrast to a distribution of distances; as discussed below a real distribution can be distinguished from under-sampling of the REDOR curve. The width of the Gaussian, hence standard deviation in calculated distance, is less than 0.1 Å. This can be further improved by sampling more points within this range of λ_D as shown in the bottom panel of Figure 2 for a spacing between REDOR data points of $\Delta(\lambda_D) = 0.036$. Distributions from further data truncation tend to become more asymmetric, averaging to lower dipolar couplings/longer distances, but skewed such that the mode is at shorter distances.

Sampling Intervals. Often it is necessary to compromise between the number of REDOR data points and higher signal-to-noise. Therefore it is instructive to characterize the BS-REDOR approach with respect to variable sampling intervals. A series of reconstructions (not shown) performed on data as in Figure 2 indicates no systematic accuracy or precision loss when the sampling rate is reduced from $\Delta(\lambda_D) = 0.036$ (48 points) to 0.58 (3 points) for data simulated up to $\lambda_D = 1.74$.

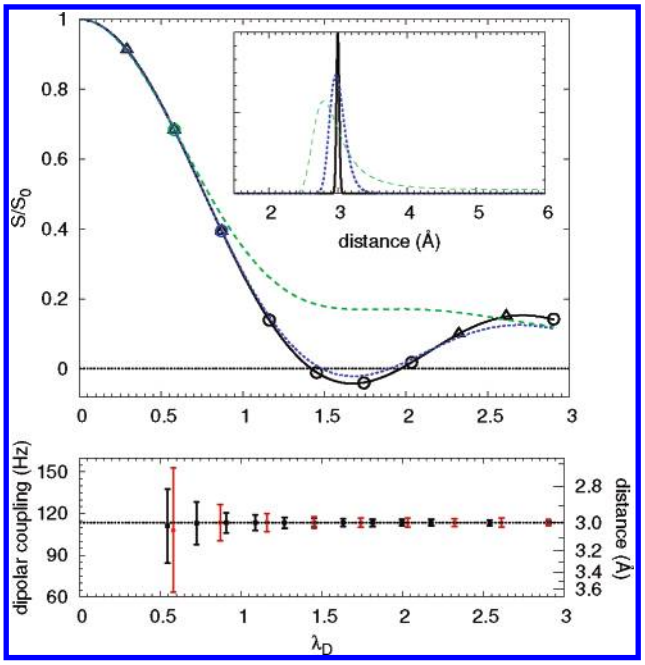

Figure 2. BS-REDOR reconstructions of model ^{13}C{^{15}N}REDOR data for a 3 Å (113 Hz) internuclear distance with a spacing between points of $\Delta(\lambda_D) = 0.29$. Reconstruction runs from 1.5 to 6 Å with a resolution of 0.01 Å. (Top) REDOR data points with corresponding positive and negative Lagrange multipliers in the reconstructions are plotted as triangles and circles, respectively. Calculated REDOR curves are shown with BS-REDOR distance distributions (inset) for data truncated at $\lambda_D = 0.58$ (green), 0.87 (blue), and 2.9 (black). As discussed in the text, these distributions represent uncertainty in the measured distance. (Bottom) Calculated distance and dipolar coupling as a function of data truncation with a spacing between data points of $\Delta(\lambda_D) = 0.29$ (red) and $\Delta(\lambda_D) = 0.036$ (black). Standard deviation is plotted as error bars about the mean.

It becomes easy to believe that only a few data points are necessary to reconstruct a single discrete distance with relatively high precision. To assess the minimum number of data points required for an accurate and precise reconstruction, BS-REDOR analysis was performed on two fixed data points at $\lambda_D = 0.29$ and 2.9 to loosely anchor the dephasing curve at each end while varying the position of a third data point (Figure 3). Results are extremely sensitive to the position of the third data point. Data points between $\lambda_D = 1.45$ to 1.74, corresponding to approximately the center of the first oscillation, have the greatest impact on precisely identifying the correct internuclear distance. When the data point is moved earlier than this range the loss of accuracy and precision is similar to the heavily truncated data in Figure 2. When positioned at times longer than this range, the analysis finds a bimodal distribution for which the floating data point *is* within the range of $\lambda_D = 1.45$ to 1.74. The broad Gaussian-like distribution at longer distance corresponds to a damped dephasing curve and the fixed data point at $\lambda_D = 0.29$ manifests as a minor peak at shorter distance.

The limits of the BS-REDOR analysis were further tested using just one or two data points from a discrete 3 Å distance (not shown). Using the $\lambda_D = 0.29$ data point as the sole constraint results in the relative absence of distribution density at short distances. However, the distance distribution builds

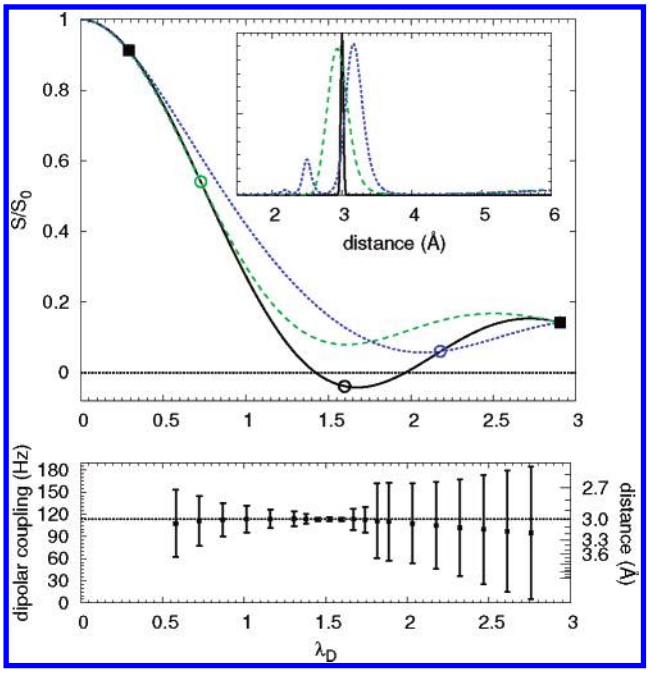

Figure 3. BS-REDOR reconstructions of the same $^{13}C-^{15}N$ distance and plotted using the same conventions as in Figure 2. Each reconstruction used only three REDOR data points, two points held constant at $\lambda_D = 0.29$ and 2.9 with the third point at different positions in between. (Top) Calculated REDOR curves and corresponding distance distributions from reconstructions for a third point positioned at $\lambda_D = 0.87$ (green), 1.59 (blue), and 2.18 (black). (Bottom) Distribution statistics (as in Figure 2) for all third-point positions with steps of $\Delta(\lambda_D) = 0.145$.

rapidly between 2.0 and 3.0 Å and then increases steadily to the maximum specified distance used in the reconstruction (in this case 6 Å). Including a second data point at $\lambda_D = 0.87$ results in a distance distribution very similar to the three data point reconstruction in Figure 2 using $\lambda_D = 0.29$, 0.58 and 0.87 (blue curve). In contrast, analysis using a single data point near the first oscillation ($\lambda_D = 1.67$) results in a near-perfect distance estimate with a very narrow distribution. This is not surprising, as there are an extremely narrow range of dipolar couplings which can give rise to a data point at $S/S_0 = -0.043$.

Realistically, distances are likely to be less discrete, and reconstructions using the single $\lambda_D = 1.67$ data point from data simulated with a Gaussian distance distribution yields a number of peaks at shorter distance in addition to the "correct" distance. Hence, while a single REDOR data point is sufficient when a discrete single distance can be assumed, as expected, it is not sufficient for a distribution of distances. However, three judiciously timed data points appear to be enough to characterize less discrete internuclear distances. Reconstructions on data at $\lambda_D = 0.29$, 0.87, and 1.67 simulated from Gaussian distance distributions with standard deviation systematically varied from 0.05 to 0.25 Å (not shown) nearly perfectly reproduced the initial model distributions, diverging only at the widest distribution.

These observations indicate that unlike REDOR transforms, BS-REDOR analysis behaves similarly to nonlinear least-squares fitting, insofar as they each require data only between zero and the first oscillation for a given distance. Boltzmann maximum entropy statistics are such that distribution density will be finite at all distances within the permitted range except where the data requires either more or less density. While BS-REDOR analysis is generally more free to better fit experimental data than biased approaches, the "most probable" distribution of internuclear distances reconstructed by BS-REDOR could also be considered to reflect the maximum uncertainty in the distance measurement.

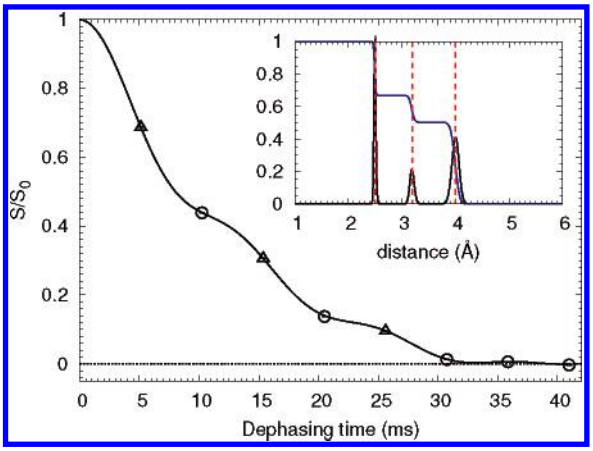

Figure 4. BS-REDOR reconstruction of model $^{13}C\{^{15}N\}$REDOR data for three distances (indicated as dotted vertical lines in the inset) described in the text and plotted as in Figure 2. Eight data points are spaced evenly from 5.12 to 41 ms. The reconstructed distances ± standard deviation with relative contributions (inset) are: 2.50 ± 0.02 Å (33.2%), 3.19 ± 0.04 Å (16.5%), and 4.00 ± 0.07 Å (50.3%). Reconstruction ran from 1 to 6 Å with 0.01 Å resolution.

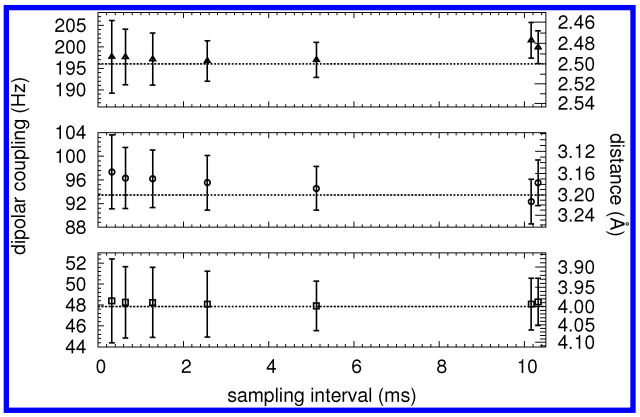

Figure 5. Distance and dipolar coupling distributions from BS-REDOR reconstructions in Figure 4 as a function of sampling interval.

Multiple Distances. Similar to earlier demonstrations of transforms on REDOR data,[67] a REDOR dephasing curve for three distinct $^{13}C-^{15}N$ distances with different relative contributions was simulated: 33.3% 2.5 Å (196.0 Hz), 16.7% 3.2 Å (93.5 Hz), and 50% 4.0 Å (47.9 Hz). The maximum dephasing time (41 ms) corresponds to $\lambda_D = 8.03$, 3.83, and 1.96 respectively for the three distances. Figure 4 shows the reconstruction using 8 evenly spaced REDOR data points. While the reconstructed accuracy, precision, and relative integrals of the distances is impressive, from the analysis of a single-distance above we expect both the 3.2 and 4 Å distance components to be narrower. Hence the presence of multiple distances slightly decreases the accuracy and precision. The 33.3% 2.5 Å distance, however, is remarkably narrow, suggesting that the broadening observed for multiple distances can be rescued by collecting data at longer dephasing times when possible.

Figure 5 summarizes the effect of reduced sampling rates on the same set of three internuclear distances. As few as four linearly spaced data points from 10.24 to 41 ms reconstructs the specified distance distribution with reasonable accuracy and precision, although this four-point reconstruction includes a cluster of false peaks at distances shorter than 2.5 Å, and taking their density from the 2.5 Å distance peak, similar to Figure 6B (discussed below). Nonlinear sampling schemes using 16 data points from 2.6 to 41 ms were also tried, and performed

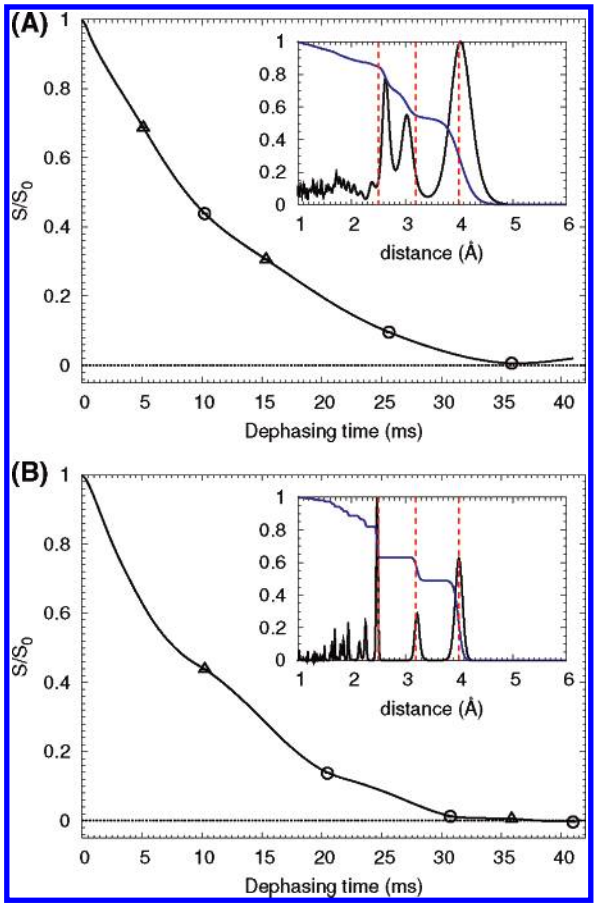

Figure 6. Secondary BS-REDOR reconstructions from the eight-point reconstruction in Figure 4, with the same plotting conventions as in Figure 2. Plots show reconstructions using the data with (A) the five highest (most positive) and (B) the five lowest (most negative) corresponding Lagrange multipliers from Figure 4.

similarly or slightly better than the 16-point linear sampling, analogous to numerous examples in NMR signal processing.[49,68−70]

The unifying principle underlying both truncation and sampling is found in the Lagrange multipliers. From eq 6, positive multipliers increase the calculated entropy (H^{REDOR}), whereas negative multipliers constrain H^{REDOR} to lower values. As clustering of density in the distance distribution amounts to reducing the maximum entropy, the data points corresponding to the smallest (most negative) Lagrange multipliers define the sharpest features in the resulting distribution.

Of the eight REDOR data points in Figure 4, the subset of five points with the largest Lagrange multipliers (varying between −15.2 and 21.3) were used for the secondary reconstruction shown in Figure 6A. Similar to the 8 data point reconstruction the shortest distance/largest coupling is defined most accurately as a more complete dephasing curve is contained within the REDOR data. The longest distance is therefore most imprecise, although still accurate by virtue of comprising 50% of the total density. The intermediate distance also loses precision but more so accuracy, which also appeared in the 8 data point reconstruction.

Figure 6B shows the conjugate reconstruction using the five data points from Figure 4 corresponding to the most negative Lagrange multipliers (varying between −97.2 and −2.0). These points again highlight the importance of the information content in data around $\lambda_D \approx 1.67$ as demonstrated previously in Figure 3. $\lambda_D \approx 1.67$ for the component 2.5, 3.2 and 4.0 Å distances correspond to approximately 8.5, 18 and 35 ms, respectively. Significantly, the data points closest to these dephasing times correspond to the negative Lagrange multipliers (plotted as circles) in Figure 4. In contrast to Figure 6A, all three components are as accurate and precise as the original eight-point reconstruction in Figure 4. The first data point in both reconstructions is at 10.24 ms and a cluster of false density appears at short distances. The decrease in maximum entropy per point from the negative set of Lagrange multipliers (Figure 6B) corresponds to observed precision in the distance distributions.

In the reconstructions of Figure 2, the negative Lagrange multipliers are observed where the dephasing is near zero. In other reconstructions of a single but variable discrete distance using 13 to 25 data points extending to about $\lambda_D = 2.0$ (not shown), negative Lagrange multipliers dominate between $\lambda_D =$ 1.2 and 2.0. This corresponds to the first oscillation in the REDOR dephasing curve (Figure 1), the importance of which was already highlighted in Figure 3. Analogous to NMR signal detection, data in this later region is important for precision of reconstructed distances, and explains why accuracy and precision is lost upon truncation in Figure 2. The negative multipliers are not found exclusively in this region of the dephasing curve, and as might be expected, data points from initial dephasing times are also important. Importantly, points with positive Lagrange multipliers should not be categorically dropped for an apparent improvement in precision. Truncation at the beginning of the dephasing curve in the two cases of Figure 6, as well as the single-point ($\lambda_D = 1.67$) reconstruction on a single Gaussian distance distribution, above, demonstrate that the process will find the most probable distances to place distribution density; distances which contribute most where there are large gaps in the data will be presumed to have density to account for the apparent dephasing during the gap. A balance between positive and negative Lagrange multipliers appears critical for an accurate and precise reconstruction of where the distribution density both is and is not.

BS-REDOR Analysis of Experimental Data. Application of BS-REDOR to real data highlights some of the practical considerations and remaining limitations which must be kept in mind.

A scaling factor[66] γ_a must be included to compensate for incomplete isotopic enrichment or dilution of the labeled observe spin where the signal overlaps with an observe nucleus which is not coupled to a dephasing nucleus

$$\gamma_a = \frac{A_I A_S(1-f) + f A_I \epsilon_S(1-\epsilon_I) + f \epsilon_I \epsilon_S}{A_I - f A_I \epsilon_I + f \epsilon_I} \qquad (13)$$

for molecular enrichment fraction f, natural abundances A_I and A_S, and labeling efficiencies at enriched positions ϵ_I and ϵ_S for observed nucleus S and dephasing nucleus I, respectively.

Experimental REDOR data can be further attenuated owing to instrumental dependence of dephasing efficiencies,[63,71] accounted for by an additional scaling factor γ_b. The instrument-dependent scaling factor arises from effects such as finite pulse lengths and imperfect pulse shapes, etc. It is constant for a given instrument and heteronuclear spin-pair, and independent of sample. γ_b was empirically optimized by searching for the value which minimizes the final χ^2 value and systematic (nonrandom) errors of the BS-REDOR reconstruction. If γ_b is set too low, the reconstruction systematically undershoots the data at longer REDOR evolution times. Conversely, if γ_b is set too high, distance distribution density is forced into longer distances to account for apparent dephasing. Including

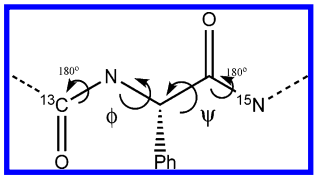

Figure 7. Dihedral angles which affect [1-^{13}C]F19-[^{15}N]A21 internuclear distance in Ac-KLVFFAE-NH_2. The distances for an α-helix and β-strand are 3.3 Å and 4.5 Å, respectively. Standard bond lengths and angles and a peptide bond dihedral angle of 180° were used.

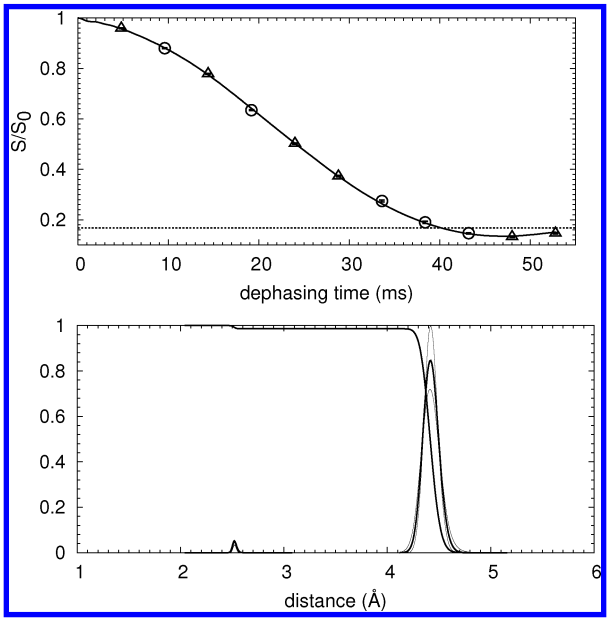

Figure 8. BS-REDOR reconstruction of ^{13}C{^{15}N}REDOR of [1-^{13}C]-F19-[^{15}N]A21 Aβ (16−22) nanotubes as described in the text. (Top) Data and reconstruction plotted as in Figure 2. The dotted line represents the asymptotic limit 1 minus the scaling factor ($\gamma_a\gamma_b = 0.833$). Data error is less than the plotted point size. (Bottom) Corresponding distance distribution. The gray region indicates the Monte Carlo averages plus and minus one standard deviation.

these terms for analysis of experimental REDOR data, eq 9 becomes

$$\overrightarrow{S/S_0} = (1 - \gamma_a\gamma_b) + \frac{\gamma_a\gamma_b}{Z}\mathscr{R}\vec{l} \qquad (14)$$

Aβ (16−22) Nanotubes. BS-REDOR analysis was tested on a relatively long (>4 Å) ^{13}C−^{15}N distance in the amyloid forming peptide Aβ(16−22), CH_3CO-KLVFFAE-NH_2. This peptide comprises the core segment of the amyloid forming Aβ-(1−42) peptide of Alzheimer's disease[72−76] and at acidic pH Aβ(16−22) self-assembles into β-sheet-rich homogeneous peptide nanotubes.[77] The distance between the carbonyl carbon of F19 and the nitrogen of A21 (Figure 7) is sensitive to the dihedral angle configuration of F20 and is consequently indicative of secondary structure.

BS-REDOR analysis of the ^{13}C{^{15}N}REDOR data in Figure 8 employs scaling factors of $\gamma_a = 1.0$ and $\gamma_b = 0.833$. Although not shown explicitly in Figure 8, 1.1% of total intensity is fixed at 1.33 Å in the reconstruction owing to spectral overlap of the natural abundance F20 carbonyl carbon with the enriched F19 signal. Greater than 98% of the [1-^{13}C]F19-[^{15}N]A21 internuclear distribution density is found in a relatively narrow peak at 4.43 Å (Figure 8). As the dephasing data extended through the first oscillation to $\lambda_D = 1.86$, and as BS-REDOR analysis calculates the widest possible distribution consistent with the data, the narrow distribution, ±0.1 Å at half-maximum, suggests

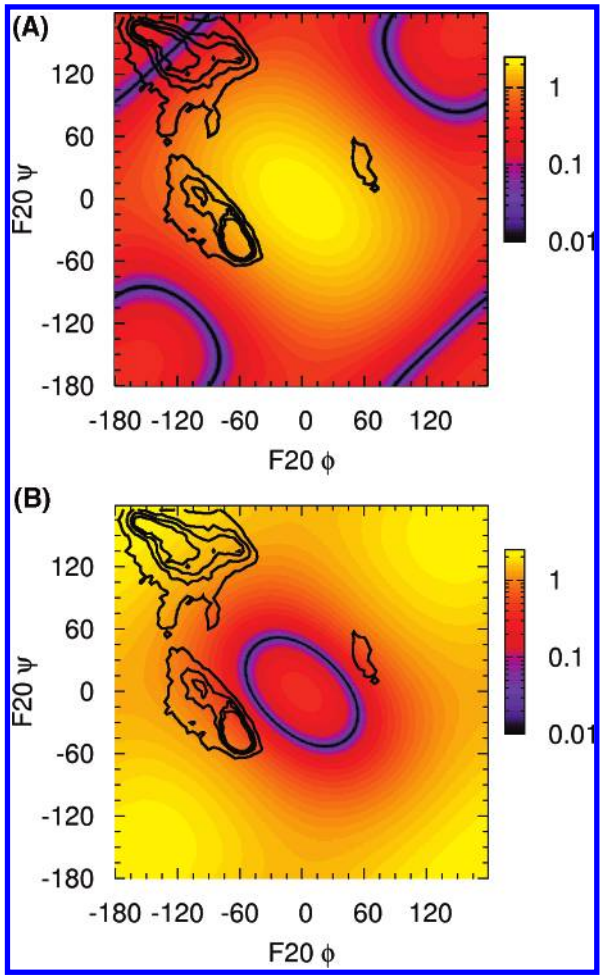

Figure 9. Deviation of [1-^{13}C]F19-[^{15}N]A21 internuclear distance (in Å), owing to variation in F20 ϕ and ψ dihedral angles, from (A) 4.36 Å and (B) 2.49 Å. Darkest coloring represents the best fit. Peptide bond dihedral angles are fixed at 180°. Both plots are overlaid with phenylalanine ϕ, ψ dihedral angle contours[87] (black). Contours surrounding (ϕ,ψ) angles of approximately (−130°,140°) correspond to a β-strand conformation, angles of approximately (−60°,−45°) correspond to a right-handed α-helix, and (60°,45°) correspond to a left-handed helix.

very high sample order. The Monte Carlo statistical variation in the distribution using root-mean-square of noise variation in the data indicates that the distribution density remains centered at 4.43 Å with a barely perceptible potential decrease in precision.

To account for molecular libration, measured dipolar couplings are increased by 5%, or equivalently distances are reduced by 1.7%,[78,79] making the reconstructed 4.43 Å distance for [1-^{13}C]F19-[^{15}N]A21 4.36 Å. The deviation of the REDOR determined distance from calculated distances as a function of the F20 dihedral angles is shown in Figure 9. A minima is found coinciding with phenylalanine dihedral angles in the PDB corresponding to β-strand conformation of (ϕ, ψ) ≈ (−128,-140), consistent with the proposed model[77] and CD, IR, and X-ray powder diffraction showing that the peptide adopts a β-strand conformation.

An artifact with very minor distribution density is also observed in Figure 8 at 2.5 Å. As in the application of Shannon maximum entropy to NMR spectral processing,[47,48] potential "false positive" peaks such as this must be investigated on a case-by-case basis. In this case the 2.5 Å peak is a consequence of the magnitude of data error; if errors are artificially increased, an additional similarly minor peak appears at approximately 3.5

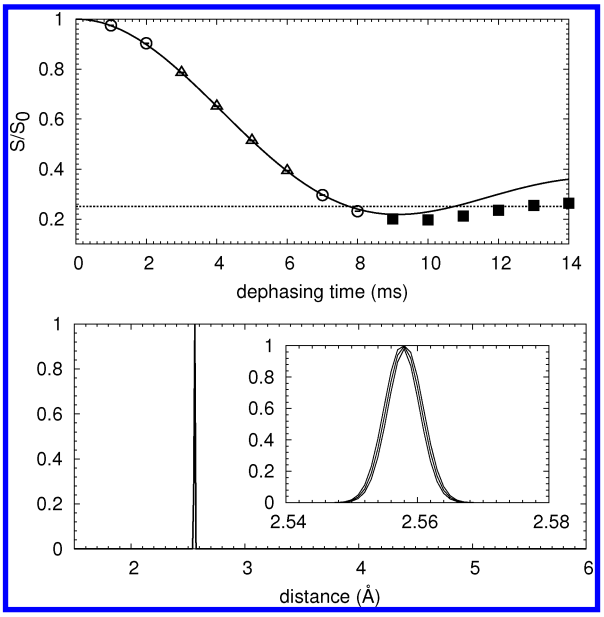

Figure 10. BS-REDOR reconstruction of $^{13}C\{^{15}N\}$REDOR for diluted [1-^{13}C,^{15}N]glycine (black), using $\gamma_a\gamma_b = 0.749$ (see text) and restricting distances from 1.5 to 6 Å with 0.01 Å resolution. Data plotted as in Figure 2. Solid squares indicate excluded data. Data error is less than the plotted point size. Monte Carlo averages ± standard deviations are shown in gray for a second reconstruction restricted from 2 to 3 Å with 0.001 Å resolution (inset).

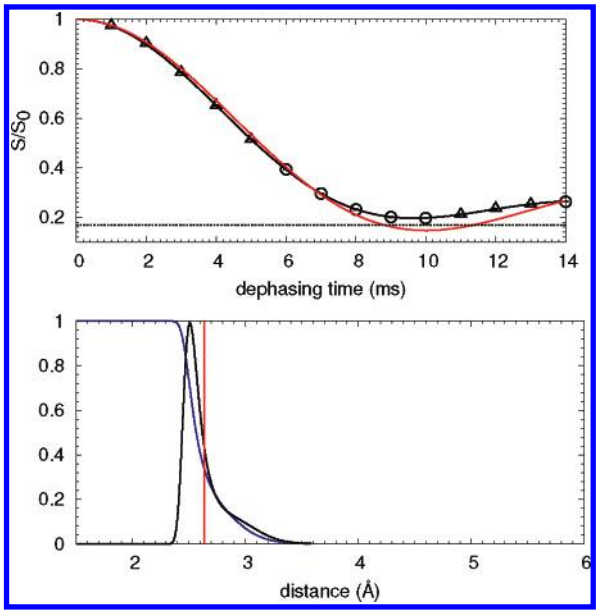

Figure 11. BS-REDOR reconstruction as in Figure 10 but extending data to 14 ms and empirically optimized $\gamma_a\gamma_b = 0.818$. Monte Carlo averages ± standard deviations are indistinguishable from the reconstruction. A simulated REDOR curve for 2.64 Å distance, the mean of the corresponding distance distribution (lower), is also plotted in red.

Å. The 2.5 Å distance is inconsistent with intramolecular contacts, owing to the steric hindrance of F20 dihedral angles required to explain the 2.5 Å distance (Figure 9B) and is unlikely to correspond to an intermolecular contact.

α-Glycine. The fixed distance within [1-^{13}C, ^{15}N] glycine is commonly used for setup of REDOR. Typically the sample is diluted to 10% by recrystallization with unlabeled glycine to reduce complications from intermolecular heteronuclear contacts. These multiple spin effects are not completely eliminated, a complication commonly disregarded in analysis. Application of BS-REDOR to this data illustrates the behavior which may indicate the presence of unexpected multiple spin effects.

Figure 10 shows a reconstruction using $\gamma_a = 0.9$ from eq 13 with ϵ_I and $\epsilon_S = 0.99$ and $f = 0.10$ and $\gamma_b = 0.833$ as for the Aβ nanotubes. When data is truncated at 8 ms, BS-REDOR reveals a distance of 2.56 Å. Adjusted for libration to 2.52 Å, this distance is just 1−2% longer than the crystallographic distance of 2.48 Å.[80]

However, when $^{13}C\{^{15}N\}$REDOR data on 10% glycine is extended to longer evolution times BS-REDOR gives nonphysical distributions. Empirically optimized scaling factors move toward 1.0, and the distance distributions become less precise with increasing mean. Figure 11 shows a reconstruction on data up to 14 ms with $\gamma_a\gamma_b = 0.818$. Approximately 80% of the distance distribution intensity is found in a relatively narrow Gaussian-like feature centered at 2.52 Å but with a tailing of remaining density to longer distances, causing the mean of the distribution to increase to 2.64.

The need to truncate data, or to adopt convenient scaling factors, is a consequence of the dilution for labeled glycine. While recrystallization with natural abundance glycine reduces the effects of intermolecular dipolar couplings, finite probability remains that crystallographic nearest neighbors will also be isotopically enriched. In α-glycine several of these potential intermolecular carbonyl carbon to nitrogen distances are significantly short,[80] 3.46, 3.59, 3.71, 3.92, and 3.94 Å, with all other nearest neighbor distances greater than 4.8 Å. In the diluted sample, only a $0.9^4 = 66\%$ of the intramolecular $^{13}C\{^{15}N\}$-REDOR signal will be unaffected by these neighboring molecules. The remaining fraction will have the added complication of the coupling of a single observed ^{13}C spin to multiple ^{15}N spins.[67,81−86] Consequently, the isolated spin-pair condition for BS-REDOR expressed by eq 2 is not completely satisfied. Nevertheless, the 2.52 Å determined with truncated data at approximately the first oscillation is consistent with the previously identified tendency for multiple spin effects to cause a slight overestimation of distance using data in the limit of short dephasing time.[81] When including more information on the multiple-spin effects inherent in additional time points, BS-REDOR still identifies the principal internuclear contact with reasonable accuracy and precision.

Conclusion

BS-REDOR analysis performs admirably in reconstructing unbiased yet reasonably accurate and precise distance distributions from experimentally feasible limited REDOR data sets. While data from the inherently error-sensitive frequency-specific first oscillation of the REDOR dephasing curve is very important, only a few points in the region are sufficient. These points together with data extending back to zero dephasing time provide all the information necessary for analysis. Application of BS-REDOR together with an understanding of the information content of each data point can guide the spectroscopist in real time during the acquisition, allowing limited experimental time to be spent gaining better signal-to-noise for chosen time points. This principle is best illustrated by the demonstrations of BS-REDOR on model data together with application of the analysis on Aβ nanotubes. Many fewer points could have described the distance distribution in the latter, and the experimental time spent instead on better signal-to-noise to remove the short-length artifact.

Owing to the complexity of configuration space with respect to the Lagrange multipliers and the current heuristic search method for finding them, the analysis is most robust when limited to approximately 16−20 points. However, care should be taken that experimental imperfections are not manifest as

real density. Regardless, a good reconstruction provides the most probable distance distribution consistent with the data and realistic estimates of data error. The method is also robust enough to reveal the presence of multiple distances, depending upon the information content of the data. Further work is necessary to expand the BS-REDOR approach beyond its current applicability to isolated spin pairs.

Acknowledgment. F.S. thanks the ARC for financial support, and A.K.M. and K.L. are grateful to David Lynn (Emory University) for encouragement and support.

References and Notes

(1) Gullion, T.; Schaefer, J. *J. Magn. Reson.* **1989**, *81*, 196−200.
(2) Gullion, T.; Schaefer, J. *Adv. Magn. Reson.* **1989**, *13*, 57−83.
(3) Macholl, S.; Sack, I.; Limbach, H.-H.; Pauli, J.; Kelly, M.; Buntkowsky, G. *Magn. Reson. Chem.* **2000**, *38*, 596−603.
(4) Murphy, O. J.; Kovacs, F. A.; Sicard, E. L.; Thompson, L. K. *Biochemistry* **2001**, *40*, 1358−1366.
(5) Garbow, J. R.; McWherter, C. A. *J. Am. Chem. Soc.* **1993**, *115*, 238−244.
(6) Sack, I.; Balazs, Y. S.; Rahimipour, S.; Vega, S. *J. Magn. Reson.* **2001**, *148*, 104−114.
(7) Seebach, D.; Sifferlen, T.; Bierbaum, D. J.; Rueping, M.; Jaun, B.; Schweizer, B.; Schaefer, J.; Mehta, A. K.; O'Connor, R. D.; Meier, B. H.; Ernst, M.; Glattli, A. *Helv. Chim. Acta* **2002**, *85*, 2877−2917.
(8) Yang, J.; Weliky, D. P. *Biochemistry* **2003**, *42*, 11879−11890.
(9) Bernard, G. M.; Miskolzie, M.; Kotovych, G.; Wasylishen, R. E. *Can. J. Chem* **2004**, *82*, 1554−1563.
(10) Olsen, G. L.; Edwards, T. E.; Deka, P.; Varani, G.; Sigurdsson, S. T.; Drobny, G. P. *Nucleic Acids Res.* **2005**, *33*, 3447−3454.
(11) Smith, S. O.; Smith, C.; Shekar, S.; Peersen, O.; Ziliox, M.; Aimoto, S. *Biochemistry* **2002**, *41*, 9321−9332.
(12) Nishimura, K.; Kim, S.; Zhang, L.; Cross, T. A. *Biochemistry* **2002**, *41*, 13170−13177.
(13) Hughes, E.; Middleton, D. A. *J. Biol. Chem.* **2003**, *278*, 20835−20842.
(14) Toke, O.; Maloy, W. L.; Kim, S. J.; Blazyk, J.; Schaefer, J. *Biophys. J.* **2004**, *87*, 662−674.
(15) Mani, R.; Tang, M.; Wu, X.; Buffy, J. J.; Waring, A. J.; Sherman, M. A.; Hong, M. *Biochemistry* **2006**, *45*, 8341−8349.
(16) Porcelli, F.; Buck-Koehntop, B. A.; Thennarasu, S.; Ramamoorthy, A.; Veglia, G. *Biochemistry* **2006**, *45*, 5793−5799.
(17) Wang, J.; Balazs, Y. S.; Thompson, L. K. *Biochemistry* **1997**, *36*, 1699−1703.
(18) Kaustov, L.; Kababya, S.; Du, S.; Baasov, T.; Gropper, S.; Shoham, Y.; Schmidt, A. *Biochemistry* **2000**, *39*, 14865−14876.
(19) Balbach, J. J.; Yang, J. J.; Weliky, D. P.; Steinbach, P.; Tugarinov, V.; Anglister, J.; Tycko, R. *J. Biomol. NMR* **2000**, *16*, 313−327.
(20) Li, Y. K.; Poliks, B.; Cegelski, L.; Poliks, M.; Gryczynski, Z.; Piszczek, G.; Jagtap, P. G.; Studelska, D. R.; Kingston, D. G. I.; Schaefer, J.; Bane, S. *Biochemistry* **2000**, *39*, 281−291.
(21) Watts, J. A.; Watts, A.; Middleton, D. A. *J. Biol. Chem.* **2001**, *276*, 43197−43204.
(22) Mehta, A. K.; Studelska, D. R.; Fischer, M.; Giessauf, A.; Kemter, K.; Bacher, A.; Cushman, M.; Schaefer, J. *J. Org. Chem.* **2002**, *67*, 2087−2092.
(23) Smith, S. O.; Eilers, M.; Song, D.; Crocker, E.; Yang, W.; Groesbeek, M.; Metz, G.; Ziliox, M.; Aimoto, S. *Biophys. J.* **2002**, *82*, 2476−2486.
(24) Kaustov, L.; Kababya, S.; Belakhov, V.; Baasov, T.; Shoham, Y.; Schmidt, A. *J. Am. Chem. Soc.* **2003**, *125*, 4662−4669.
(25) Getmanova, E.; Patel, A. B.; Klein-Seetharaman, J.; Loewen, M. C.; Reeves, P. J.; Friedman, N.; Sheves, M.; Smith, S. O.; Khorana, H. G. *Biochemistry* **2004**, *43*, 1126−1133.
(26) Mehta, A. K.; Shayo, Y.; Vankayalapti, H.; Hurley, L. H.; Schaefer, J. *Biochemistry* **2004**, *43*, 11953−11958.
(27) Tycko, R. *Annu. Rev. Phys. Chem.* **2001**, *52*, 575−606.
(28) Jaroniec, C. P.; MacPhee, C. E.; Astrof, N. S.; Dobson, C. M.; Griffin, R. G. *Proc. Natl. Acad. Sci. U.S.A.* **2002**, *99*, 16748−16753.
(29) Naito, A.; Kamihira, M.; Inoue, R.; Saito, H. *Magn. Reson. Chem.* **2004**, *42*, 247−257.
(30) Kao, H. M.; O'Connor, R. D.; Mehta, A. K.; Huang, H. Y.; Poliks, B.; Wooley, K. L.; Schaefer, J. *Macromolecules* **2001**, *34*, 544−546.
(31) Hou, S. S.; Beyer, F. L.; Schmidt-Rohr, K. *Solid State Nucl. Magn. Reson.* **2002**, *22*, 110−127.
(32) Fechtelkord, M.; Behrens, H.; Holtz, F.; Bretherton, J. L.; Fyfe, C. A.; Groat, L. A.; Raudsepp, M. *Am. Mineral.* **2003**, *88*, 1046−1054.
(33) Fry, R. A.; Kwon, K. D.; Komarneni, S.; Kubicki, J. D.; Mueller, K. T. *Langmuir* **2006**, *22*, 9281−9286.
(34) Andrew, E. R.; Bradbury, A.; Eades, R. G. *Nature* **1958**, *182*, 1659.
(35) Lowe, I. J. *Phys. Rev. Lett.* **1959**, *2*, 285.
(36) Mueller, K. T. *J. Magn. Reson. A* **1995**, *113*, 81−93.
(37) Gullion, T.; Kishore, R.; Asakura, T. *J. Am. Chem. Soc.* **2003**, *125*, 7510−7511.
(38) Arshava, B.; Breslav, M.; Antohi, O.; Stark, R. E.; Garbow, J. R.; Becker, J. M.; Naider, F. *Solid State Nucl. Magn. Reson.* **1999**, *14*, 117−136.
(39) Kim, S. J.; Cegelski, L.; Studelska, D. R.; O'Connor, R. D.; Mehta, A. K.; Schaefer, J. *Biochemistry* **2002**, *41*, 6967−6977.
(40) Gibson, J. M.; Raghunathan, V.; Popham, J. M.; Clayton, P. S.; Drobny, G. *J. Am. Chem. Soc.* **2005**, *127*, 9350−9351.
(41) Mueller, K. T.; Jarvie, T. P.; Aurenta, D. J.; Roberts, B. W. *Chem. Phys. Lett.* **1995**, *242*, 535−542.
(42) Bertani, P.; Raya, J.; Hirschinger, J. *Solid State Nucl. Magn. Reson.* **2002**, *22*, 188−203.
(43) d'Espinose de la Caillerie, J.-B.; Fretigny, C. *J. Magn. Reson.* **1998**, *133*, 273−280.
(44) Jarvie, T. P.; Went, G. T.; Mueller, K. T. *J. Am. Chem. Soc.* **1996**, *118*, 5330−5331.
(45) Schäfer, H.; Sternin, E. *Phys. Can.* **1997**, *77*−85.
(46) Vogt, F. G.; Aurentz, D. J.; Mueller, K. T. *Mol. Phys.* **1998**, *95*, 907−919.
(47) Hoch, J. C.; Stern, A. S.; Donoho, D. L.; Johnstone, I. M. *J. Magn. Reson.* **1990**, *86*, 236−246.
(48) Hoch, J. C.; Stern, A. S. *Methods Enzymol.* **2001**, *338*, 159−178.
(49) Jones, D. N.; Opella, S. J. *J. Magn. Reson.* **2006**, *179*, 105−113.
(50) Shannon, C. E. *Bell Syst. Tech. J.* **1948**, *27*, 379−423.
(51) Pan, Y.; Gullion, T.; Schaefer, J. *J. Magn. Reson.* **1990**, *90*, 330−340.
(52) Li, Y.; Evans, J. *J. Chem. Phys.* **1994**, *101*, 10211−10216.
(53) Bevensee, R. M. *Maximum Entropy Solutions to Scientific Problems*; Prentice Hall: Englewood Cliffs, NJ, 1993 (ISBN 0-13-563818-6).
(54) Ernst, R. R.; Bodenhausen, G.; Wokaun, A. *Principles of Nuclear Magnetic Resonance in One and Two Dimensions*; Oxford Science Publications: New York, 1992.
(55) *Modern Heuristic Search Methods*; Rayward-Smith, V., Osman, I. H., Reeves, C. R., Smith, G. D., Eds.; Wiley: Chichester, New York, 1996 (ISBN 0-471-96280-5).
(56) Galassi, M.; Davies, J.; Theiler, J.; Gough, B.; Jungman, G.; Booth, M.; Rossi, F. *The GNU Scientific Library*; Network Theory: Bristol, U.K., 2003 (ISBN 0-954-16173-4).
(57) Gehman, J. D.; Paulson, E. K.; Zilm, K. W. *J. Biomol. NMR* **2003**, *27*, 235−259.
(58) Hamming, R. W. *Numerical Methods for Scientists and Engineers*, 2nd ed.; Dover Publications: New York, 1986 (ISBN 0-486-65241-6).
(59) Stejskal, E. O.; Schaefer, J.; Waugh, J. S. *J. Magn. Reson.* **1977**, *28*, 105−112.
(60) Gullion, T.; Baker, D. B.; Conradi, M. S. *J. Magn. Reson.* **1990**, *89*, 479−484.
(61) Gullion, T.; Schaefer, J. *J. Magn. Reson.* **1991**, *92*, 439−442.
(62) Rance, M.; Byrd, R. A. *J. Magn. Reson.* **1983**, *52*, 221−240.
(63) Sinha, N.; Schmidt-Rohr, K.; Hong, M. *J. Magn. Reson.* **2004**, *168*, 358−365.
(64) Fung, B. M.; Khitrin, A. K.; Ermolaev, K. *J. Magn. Reson.* **2000**, *142*, 97−101.
(65) Andrew, E. R.; Bradbury, A.; Eades, R. G.; Wynn, V. T. *Phys. Lett.* **1963**, *4*, 99−100.
(66) Jaroniec, C. P.; Tounge, B. A.; Rienstra, C. M.; Herzfeld, J.; Griffin, R. G. *J. Magn. Reson.* **2000**, *146*, 132−139.
(67) Vogt, F. G.; Mattingly, S. M.; Gibson, J. M.; Mueller, K. T. *J. Magn. Reson.* **2000**, *147*, 26−35.
(68) Stern, A. S.; Li, K.-B.; Hoch, J. C. *J. Am. Chem. Soc.* **2002**, *124*, 1982−1993.
(69) Rovnyak, D.; Filip, C.; Itin, B.; Stern, A. S.; Wagner, G.; Griffin, R. G.; Hoch, J. C. *J. Magn. Reson.* **2003**, *161*, 43−55.
(70) Rovnyak, D.; Frueh, P. D.; Sastry, M.; Sun, Z.-Y. J.; Stern, A. S.; Hoch, J. C.; Wagner, G. *J. Magn. Reson.* **2004**, *170*, 15−21.
(71) Weldeghiorghis, T. K.; Schaefer, J. *J. Magn. Reson.* **2003**, *165*, 230−236.
(72) Hilbich, C.; Kisters-Woike, B.; Reed, J.; Masters, C. L.; Beyreuther, K. *J. Mol. Biol.* **1991**, *218*, 149−163.
(73) Hilbich, C.; Kisters-Woike, B.; Reed, J.; Masters, C. L.; Beyreuther, K. *J. Mol. Biol.* **1992**, *228*, 460−473.
(74) Wood, S. J.; Wetzel, R.; Martin, J. D.; Hurle, M. R. *Biochemistry* **1995**, *34*, 724−730.
(75) Tjernberg, L. O.; Naslund, J.; Lindqvist, F.; Johansson, J.; Karlstrom, A. R.; Thyberg, J.; Terenius, L.; Nordstedt, C. *J. Biol. Chem.* **1996**, *271*, 8545−8548.
(76) Fay, D. S.; Fluet, A.; Johnson, C. J.; Link, C. D. *J. Neurochem.* **1998**, *71*, 1616−1625.

(77) Lu, K.; Jacob, J.; Thiyagarajan, P.; Conticello, V. P.; Lynn, D. G. *J. Am. Chem. Soc.* **2003**, *125*, 6391−6393.
(78) McDowell, L. M.; Klug, C. A.; Beusen, D. D.; Schaefer, J. *Biochemistry* **1996**, *35*, 5395−5403.
(79) Ishii, Y.; Terao, T.; Hayashi, S. *J. Chem. Phys.* **1997**, *107*, 2760−2774.
(80) Marsh, R. E. *Acta Crystallogr.* **1958**, *11*, 654−663.
(81) Bertmer, M.; Eckert, H. *Solid State Nucl. Magn. Reson.* **1999**, *15*, 139−152.
(82) Fyfe, C. A.; Lewis, A. R. *J. Phys. Chem. B* **2000**, *104*, 48−55.
(83) Gullion, T.; Pennington, C. H. *Chem. Phys. Lett.* **1998**, *290*, 88−93.
(84) Leppert, J.; Heise, B.; Ramachandran, R. *J. Biomol. NMR* **2000**, *18*, 153−164.
(85) Liivak, O.; Zax, D. B. *J. Chem. Phys.* **2001**, *115*, 402−409.
(86) Liivak, O.; Zax, D. B. *J. Chem. Phys.* **2000**, *113*, 1088−1096.
(87) Dayalan, S.; Gooneratne, N.; Bevinakoppa, S.; Schroder, H. *Bioinformation* **2006**, *1*, 78−80.